MOLECULAR IMAGING AND BIOLOGY

Mol Imaging Biol (2019) 21:391–398
DOI: 10.1007/s11307-018-1226-7

Published Online: 18 June 2018

RESEARCH ARTICLE

Mapping Bone Marrow Response in the Vertebral Column by Positron Emission Tomography Following Radiotherapy and Erlotinib Therapy of Lung Cancer

Azadeh Abravan,[1,2] Hanne Astrid Eide,[3,4] Ayca Muftuler Løndalen,[5] Åslaug Helland,[3,4,6] Eirik Malinen[1,2]

[1]*Department of Medical Physics, Oslo University Hospital, PO Box 4953, Nydalen, N-0424, Oslo, Norway*
[2]*Department of Physics, University of Oslo, Oslo, Norway*
[3]*Department of Oncology, Oslo University Hospital, Oslo, Norway*
[4]*Institute for Cancer Research, Oslo University Hospital, Oslo, Norway*
[5]*Department of Radiology and Nuclear Medicine, Oslo University Hospital, Oslo, Norway*
[6]*Institute of Clinical Medicine, University of Oslo, Oslo, Norway*

Abstract

Purpose: To map functional bone marrow (BM) by 2-deoxy-2-[^{18}F]fluoro-D-glucose ([^{18}F]FDG) positron emission tomography (PET) in the vertebral column of lung cancer patients prior to, during, and after treatment. Moreover, to identify radiation- and erlotinib-induced changes in the BM.

Procedures: Twenty-six patients with advanced non-small cell lung cancer, receiving radiotherapy (RT) alone or concomitantly with erlotinib, were examined by [^{18}F]FDG PET before, during, and after treatment. A total of 61 [^{18}F]FDG PET scans were analyzed. Vertebral column BM [^{18}F]FDG standardized uptake value normalized to the liver (SUV_{BMLR}) was used as uptake measure. Wilcoxon signed-rank test was used to assess changes in BM uptake of [^{18}F]FDG between sessions. Effects of erlotinib on the BM activity during and after treatment were assessed using Mann-Whitney *U* test.

Results: A homogeneous uptake of [^{18}F]FDG was observed within the vertebral column prior to treatment. Mean SUV_{BMLR} (± S.E.M) in the body of thoracic vertebrae receiving a total RT dose of 10 Gy or higher was 0.64 ± 0.01, 0.56 ± 0.01, and 0.59 ± 0.01 at pre-, mid-, and post-therapy, respectively. A significant reduction in the mean SUV_{BMLR} was observed from pre- to both mid- and post-therapy ($p < 0.05$). Mean SUV_{BMLR} was significantly higher at post-therapy compared to mid-therapy for patients receiving erlotinib in addition to RT ($p < 0.05$).

Conclusions: RT reduces BM [^{18}F]FDG uptake in the vertebral column, especially in the high-dose region. Concomitant erlotinib may stimulate a recovery in BM [^{18}F]FDG uptake from mid- to post-therapy.

Trial registration: NCT02714530. Registered 10 September 2015.

Keywords: FDG-PET, Thoracic radiotherapy, Bone marrow, Vertebral column, NSCLC, Erlotinib

Electronic supplementary material The online version of this article (https://doi.org/10.1007/s11307-018-1226-7) contains supplementary material, which is available to authorized users.

Correspondence to: Azadeh Abravan; *e-mail:* azadeh.abravan@fys.uio.no

Introduction

Approximately 50 % of all cancer patients receive radiotherapy (RT) at some point during their treatment, either with curative or palliative intent [1, 2]. Nevertheless, it is virtually impossible to treat cancer with ionizing radiation without exposing healthy tissues, and preventing normal tissue damage is as important as obtaining disease control. Different normal tissues have varying metabolic profiles, depending on their cellular architecture and their response to treatment. Understanding the metabolic response in normal tissues to cancer therapy in general and RT in particular may provide early sub-clinical signs of treatment-related alterations that could develop into tissue morbidity [3, 4].

Bone marrow (BM) is a soft, dynamic tissue located in the endosteal niche of the trabecular bone cavities. Here, hematopoietic stem cells undergo symmetric and asymmetric cell divisions to maintain hematopoietic stem cells pool size and produce blood cells. Bony structures are gradually depleted of hematopoietic cells with age [5]. Adult functional BM is situated in the proximal femur, pelvic region, vertebral column, sternum, scapula, skull, and clavicle. Both the cancer and the treatment can affect BM metabolism. BM activity may change by release of various cytokines such as vascular endothelial growth factor (VEGF) and transforming growth factor-beta (TGF-β) into the circulation by tumor cells [6, 7]. Moreover, interleukin-6 (IL-6) is a known multifunctional inflammatory cytokine. IL-6 administration is known to stimulate hematopoiesis and speed up hematopoietic suppression recovery following RT [8, 9].

RT is myelosuppressive and may alter self-renewal and differentiation processes when functional BM is irradiated. These changes in the BM may further lead to changes in the blood cell counts and affect the incidence of hematologic toxicity. It has been shown that hematologic toxicity is associated with high RT dose to the thoracic vertebrae of non-small cell lung cancer (NSCLC) patients during chemoradiotherapy (CRT) [10].

Patients with advanced stage NSCLC may benefit from thoracic RT and also targeted treatment such as erlotinib therapy [11, 12]. 2-Dexoy-2-[^{18}F]fluoro-D-glucose ([^{18}F]FDG) positron emission tomography (PET) plays an important role in the diagnostics and clinical management of NSCLC [13, 14]. In addition to the usefulness of [^{18}F]FDG PET in detecting malignant tumors, [^{18}F]FDG PET may be employed to assess activity in the healthy BM, where a minor part of the injected [^{18}F]FDG is accumulated [15]. It has been shown that pre-therapy [^{18}F]FDG uptake in the BM significantly correlates with white blood cell counts in NSCLC patients [16]. In cervical and anal cancer patients treated with CRT the dose to the functionally active BM regions, defined by pre-therapy [^{18}F]FDG PET, has been shown to be a better predictor of blood cell counts and hematologic toxicity compared to bony structures as a whole [17–19]. However, one recent study on anal cancer patients treated with CRT could not validate these findings [20]. Two studies investigating [^{18}F]FDG uptake in different regions of bony structures at baseline and follow up examinations of cervical and head and neck cancer patients treated with CRT show varying degrees of BM changes following therapy [21, 22].

About 20 % of functional BM is located in the thoracic vertebrae [23]. Thus, irradiation of thoracic BM could result in BM suppression during and after therapy. There are to our knowledge no longitudinal studies assessing functional BM using [^{18}F]FDG PET during and following thoracic RT. Also, the role of targeted therapy on functional BM in cancer patients is not clear. In this work on patients with NSCLC treated with fractionated RT or RT plus concomitant erlotinib therapy, the purpose was to map functional BM by [^{18}F]FDG PET in the vertebral column prior to, during and after treatment. Moreover, the aim was to identify radiation- and erlotinib-induced changes in the BM. Using pre-therapy [^{18}F]FDG PET, we quantified variations in functional BM distribution along the vertebral column and across patients. By means of longitudinal PET scanning, we investigated how functional BM in the vertebral column responded to RT during and after treatment. The effect of erlotinib on the BM [^{18}F]FDG uptake was further evaluated in a subgroup of patients.

Materials and Methods

Study Design

Twenty-six patients with stage III–IV NSCLC were included between November 2012 and October 2016. The median age of patients was 69.5 years (range 47 to 85 years), 22 patients were male and 4 were female. All patients received thoracic RT with a total dose of 30 Gy given in 10 fractions, which was delivered using two opposed 6 MV photon beams once every weekday at a linear accelerator. A radiation field arrangement for one NSCLC patient, showing the partial exposure of the vertebral column, can be found in the Electronic Supplementary Material (ESM) Suppl. Fig. 1. By randomization, 12 patients (46 %) were assigned to receive concomitant oral erlotinib once every day (150 mg p.o.) from the day before the start of RT and during RT. No other chemotherapy was given to the patients during the treatment. The study was approved by the Regional Committee for Medical and Health Research Ethics. A written informed consent was received from all patients.

Imaging and Delineations

RT planning CT scan was done prior to treatment at a light speed ultra-scanner (GE medical systems, USA). Furthermore, at most three [^{18}F]FDG-PET/CT examinations were performed at a Biograph 16-scanner (Siemens, Germany); one prior to RT and erlotinib therapy, one at mid-therapy (after about 1 week), and one 6 weeks post-RT. The patients included underwent at least two of these [^{18}F]FDG PET

examinations. The axial reconstruction matrix was 168 × 168 with a 4-mm in-plane resolution and 3-mm slice spacing. The slice thickness was 5 mm and reconstruction was done with OSEM2D 4i8s and a 5-mm Gaussian filter. All patients fasted for at least 6 h prior to the administration of 263–445 MBq of [^{18}F]FDG. One PET scan was excluded from the analysis due to BM hyperactivity [24].

The body of the lumbar vertebrae (L1–L2), thoracic vertebrae (T1–T12), cervical vertebrae (C6–C7), and lung were delineated based on planning CT in the RT planning system (Oncentra ® External Beam, Elekta, Sweden). Due to limited field of view in the longitudinal direction, only L1–L2 and C6–C7 could be included.

Data for analyses from delineated vertebrae were collected after co-registration of planning CT, RT dose matrix, and PET series in IDL (Interactive Data Language, v 8.6, Research Systems, Boulder, CO, USA). More detail about the trial protocol and image registration can be found in the previous work [25].

Bone Marrow [^{18}F]FDG Uptake

For each available PET scan, standardized uptake value (SUV) in the vertebral body was calculated in each image voxel and further mapped along the vertebral column (Fig. 1). The uptake pattern was typically sinusoidal, with a local maximum at the center of each vertebra and a minimum uptake where the intervertebral discs are located. The mean [^{18}F]FDG uptake over the full-width half maximum of each local peak defined the vertebral column SUV_{BM}. Corresponding RT dose to each vertebra was also calculated from the DICOM RT dose matrix. Moreover, since the RT dose was mainly delivered to the thorax, we separated thoracic vertebrae into two different regions; vertebrae that are received less than 10 Gy of total RT dose (low-dose region) and vertebrae that are received more than 10 Gy of total RT dose (high-dose region). For each available PET scan, lung SUV was also calculated by averaging over all the voxel values in the delineated lung.

Bone Marrow to Liver [^{18}F]FDG Uptake Ratio

To reduce inter-patient variation in [^{18}F]FDG uptake estimates, we corrected SUV_{BM} using mean SUV of the liver [24]. The liver was always well outside the radiation fields. Mean [^{18}F]FDG uptake of the liver was obtained by defining three small cubes (9 × 9 × 9 mm each), two in the right lobe and one in the left lobe of the liver in all PET images. A further average over these three regions in the liver was performed to calculate SUV of the liver. Bone marrow to liver [^{18}F]FDG uptake ratio (SUV_{BMLR}) was then calculated by dividing SUV_{BM} by liver SUV at each session.

Cytokine Measurements

As described previously [26], serum levels of various cytokines were assessed using a multiplex bioassay (Bio-Rad, Hercules, CA, USA) in a subgroup of patients ($n = 21$). Patients' blood values were collected at pre-, mid-, and post-therapy corresponding to the PET sessions. IL-6 and VEGF were selected for further analysis due to their importance in hematopoiesis.

Statistics

Wilcoxon signed-rank test was performed when assessing changes in the mean [^{18}F]FDG uptake of different vertebral structures between sessions. Pairwise comparisons for patients examined at pre- and mid-, pre- and post-, and mid- and post-PET sessions were performed, as not all patients underwent all three PET examinations. Mann-Whitney U test was employed when comparing vertebral column SUV_{BMLR} between two treatment groups. Variation in pre-therapy SUV_{BMLR} among the vertebrae was analyzed using single factor ANOVA. Pearson correlation was used when evaluating the correlation between vertebral column SUV_{BMLR} and IL-6 and VEGF, and between vertebral column SUV and lung SUV at different sessions. Observed differences were considered to be significant when the two-tailed p value was less than 0.05. Statistical analyses were performed in R 3.3.3 (R core team, Vienna, Austria).

Results

Patient and treatment characteristics are presented in Table 1. Number of patients having pre-therapy, mid-therapy, and post-therapy [^{18}F]FDG PET scans was 20, 25, and 16, respectively. Number of patients in each treatment group

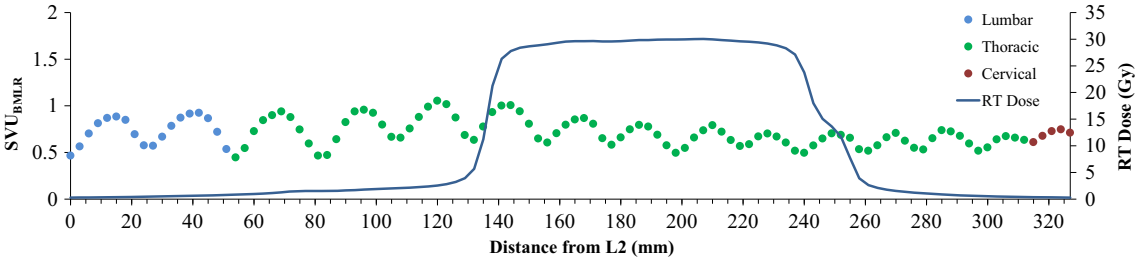

Fig. 1 Mapping of total RT dose distribution and pre-therapy vertebral column SUV corrected for liver over distance from L2 in mm.

Table 1.. Patients and treatment characteristics

	n (%/median (range))
Age (year)	69.5 (47–85)
Randomized to group	
RT	14 (54)
RT + Erlotinib	12 (46)
Gender	
Male	22 (85)
Female	4 (15)
Smoking history	
Current	7 (27)
Former	19 (73)
Stage	
III	9 (35)
IV	16 (61)
NOS	1 (4)
Histology	
Adenocarcinoma	14 (54)
Squamous cell carcinoma	10 (38)
Large cell carcinoma	2 (8)
Tumor volume (cm^3)	90.5 (2.5–648.1)
Maximum dose to VC (Gy)	30.0 (26.7–30.9)
Mean dose to VC (Gy)	9.3 (6.2–15.6)

Abbreviations: *RT* radiotherapy, *NOS* not otherwise specified, *VC* vertebral column

(RT, RT + erlotinib) at pre-, mid-, and post-therapy PET sessions was (12, 8), (14, 11) and (6, 10). Mean SUV of the liver (± SD) at pre-, mid-, and post-therapy was 2.4 ± 0.5, 2.6 ± 0.5, and 2.6 ± 0.5, respectively, based on all patients (see Suppl. Fig. 2 in ESM). There was no significant change in the liver SUV between sessions. Maximum delivered RT dose to the vertebral column ranged from 26.7 to 30.9 Gy. Mean SUV_{BMLR} (± S.E.M) in the vertebral column at pre-, mid-, and post-therapy was 0.66 ± 0.01, 0.61 ± 0.01, and 0.62 ± 0.01 respectively. Mean SUV_{BMLR} (± S.E.M) for thoracic vertebrae receiving a total RT dose of 10 Gy or more was 0.64 ± 0.01, 0.56 ± 0.01, and 0.59 ± 0.01 at pre-, mid-, and post-therapy respectively. At post-therapy, a positive correlation ($r = 0.8$, $p < 0.01$) between mean SUV in the lung and mean SUV in the vertebral column was identified for patients receiving erlotinib in addition to RT. Moreover, a significant positive association between IL-6 and vertebral column SUV_{BMLR} was identified for patients in the RT + erlotinib group ($r = 0.5$, $p = 0.01$). No significant association was seen between VEGF and vertebral column SUV_{BMLR}.

Figure 2 shows SUV_{BMLR} in each vertebra prior to treatment. As seen, SUV_{BMLR} varied little over the vertebrae and patients. Pre-therapy mean (± S.E.M) SUV_{BMLR} over all the vertebrae included in this study was 0.66 ± 0.01. No systematic variation in pre-therapy SUV_{BMLR} was seen over the vertebrae ($p = 0.2$).

Figure 3 shows sagittal planning CT images fused with the RT dose distribution and the PET images taken at pre-, mid-, and post-therapy for one patient receiving RT + erlotinib. As seen, T4–T9 was located in the high-dose region where more than 10 Gy of total RT dose was delivered. At mid-therapy, a reduction in the [^{18}F]FDG uptake of T4–T9 can be seen compared to pre-therapy. This reduction seems to be less for T4, receiving around 10 Gy, compared to T5–T9, receiving more than 20 Gy. At post-therapy, however, an increase in the [^{18}F]FDG uptake was observed for some of the vertebrae compared to mid-therapy. Comparing post-therapy to pre-therapy, a reduction in the [^{18}F]FDG uptake was still evident.

Changes in the SUV_{BMLR} for lumbar, thoracic, and cervical vertebrae, low and high RT dose, RT and RT + erlotinib group between the three PET sessions are presented in Table 2. SUV_{BMLR} of lumbar, thoracic, and cervical vertebrae at pre-, mid-, and post-therapy is shown in Fig. 4a. There was no significant change in SUV_{BMLR} of lumbar and cervical vertebrae from session to session. In the thoracic vertebrae, however, a decrease in SUV_{BMLR} from pre-therapy to both mid-therapy and post-therapy was seen. Moreover, a significant increase in SUV_{BMLR} was observed from mid- to post-therapy. Fig. 4b shows thoracic SUV_{BMLR} in the low and high RT dose regions. There was no significant change from session to session in the low-dose region. Conversely, in the high-dose region, a reduction in SUV_{BMLR} from pre- to both mid- and post-therapy was observed. A significant increase in SUV_{BMLR} from mid- to post-treatment was also seen.

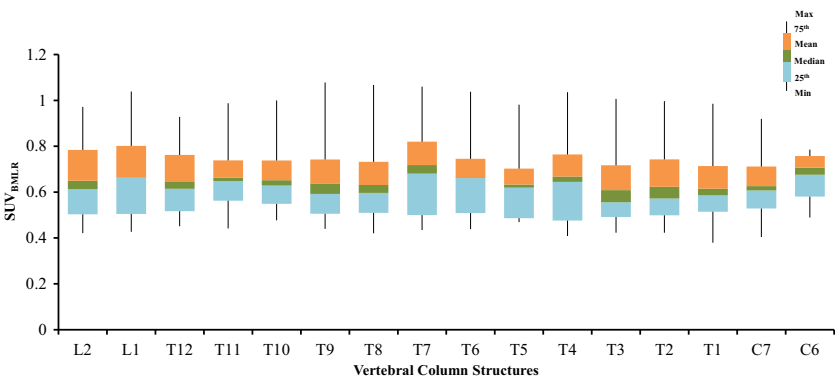

Fig. 2 Box-plot representing pre-therapy SUV_{BMLR} variation within vertebral column and across patients.

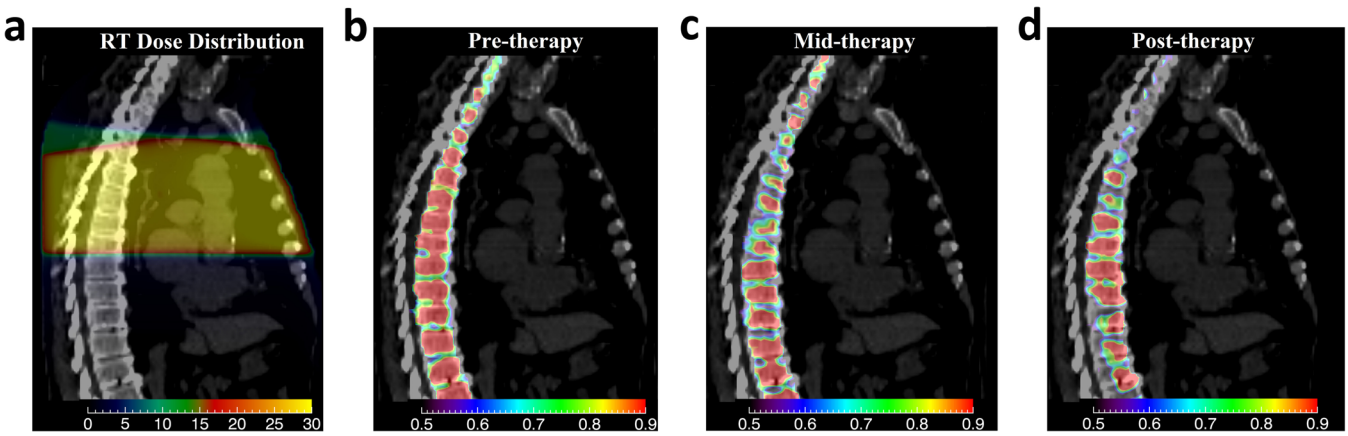

Fig. 3 From left to right: **a** planning CT fused with RT dose distribution, **b** pre-therapy PET, **c** mid-therapy PET, and **d** post-therapy PET. SUVs are corrected using liver SUV. Only PET uptake within the body of the vertebral column is displayed.

SUV_{BMLR} decreased significantly from pre- to mid- and post-therapy when including all vertebrae and both treatment groups (Fig. 4c). Moreover, SUV_{BMLR} increased 6 weeks post-treatment compared to pre-therapy. In patients treated with RT + erlotinib, a significant decrease in SUV_{BMLR} from pre- to mid- and post-therapy, and a significant increase from mid- to post-therapy were observed. Conversely, for patients treated with RT only, a decrease from pre- to mid-therapy was the only significant change in SUV_{BMLR} over the whole vertebral column. At post-therapy, vertebral column SUV_{BMLR} was significantly higher for patients in RT + erlotinib group compared to RT only ($p = 0.01$).

Table 2. Change in the SUV_{BMLR} for different structures, RT doses, and treatment groups at different time points

Structures	Change in SUV_{BMLR}		
	Mid-pre p value*	Post-pre p value*	Post-mid p value*
Lumbar	0.019 0.6	0.013 0.6	− 0.005 0.09
Thoracic	− 0.044 *< 0.01*	− 0.036 *0.01*	0.007 *0.01*
Cervical	0.048 0.1	0.045 0.8	− 0.002 0.3
Thoracic D < 10 Gy	− 0.012 0.5	− 0.023 0.2	− 0.011 0.2
Thoracic D > 10 Gy	− 0.077 *< 0.01*	− 0.049 *0.03*	0.028 *0.02*
Vertebral column (All)	− 0.047 *< 0.01*	− 0.041 *< 0.01*	0.006 *0.01*
Vertebral column (RT + erlotinib)	− 0.037 *< 0.01*	− 0.009 *< 0.01*	0.028 *< 0.01*
Vertebral column (RT)	− 0.026 *0.01*	− 0.060 0.9	− 0.034 0.7

Abbreviations: *SUV_{BMLR}* bone marrow standardized uptake value normalized to liver, *RT* radiotherapy
*p values calculated from Wilcoxon signed-rank test comparing mean changes in SUV_{BMLR} from pre-therapy to mid- and post-therapy and also from mid- to post-therapy

Discussion

BM consisting of hematopoietic cells should be spared when possible during RT [27]. The functional part of the BM is highly sensitive to radiation and subsequent decrease in [^{18}F]FDG uptake may be a result of functional BM suppression [28]. To our knowledge, this is the first longitudinal study assessing [^{18}F]FDG uptake of the BM during and following thoracic RT. We observed the distribution of functional BM within the body of vertebral column to be rather homogeneous based on [^{18}F]FDG uptake prior to treatment. Thus, there are no parts of the vertebral column to be preferably avoided during RT to minimize the potential risk of hematologic toxicity.

Yagi, et al. [21] reported a significant decrease in the T1 [^{18}F]FDG uptake after both 5- and 14-month follow-up in 14 patients with head and neck cancer treated with CRT. However, [^{18}F]FDG uptake in only one thoracic vertebra was analyzed and there was no information about total RT dose or dose delivered to different regions. Moreover, the same study found no changes in the T1 [^{18}F]FDG uptake after CRT for 18 cervical cancer patients. Also, Noticewala, et al. [22] reported that [^{18}F]FDG uptake in the thoracic vertebrae did not change from baseline to 1.5–6 months after CRT for 39 patients with cervical cancer treated with CRT. In the high-dose region, however, they reported a significant decrease (18 %) in the lumbar vertebrae (L1–L4) [^{18}F]FDG uptake post-treatment for all patients. In our study, a significant decrease (11 %) in the SUV_{BMLR} in the high-dose region of the thoracic vertebrae was observed already after 1-week of RT that could point to the same RT-induced BM suppression as the study by Noticewala, et al. [22].

In the current work, we saw clear trends in how the vertebral column uptake of [^{18}F]FDG changed during and after treatment. These trends were particularly pronounced for thoracic vertebrae that received a total dose of 10 Gy or higher. First, after 1 week of therapy, a reduction in BM metabolism (SUV_{BMLR}) was observed compared to pre-

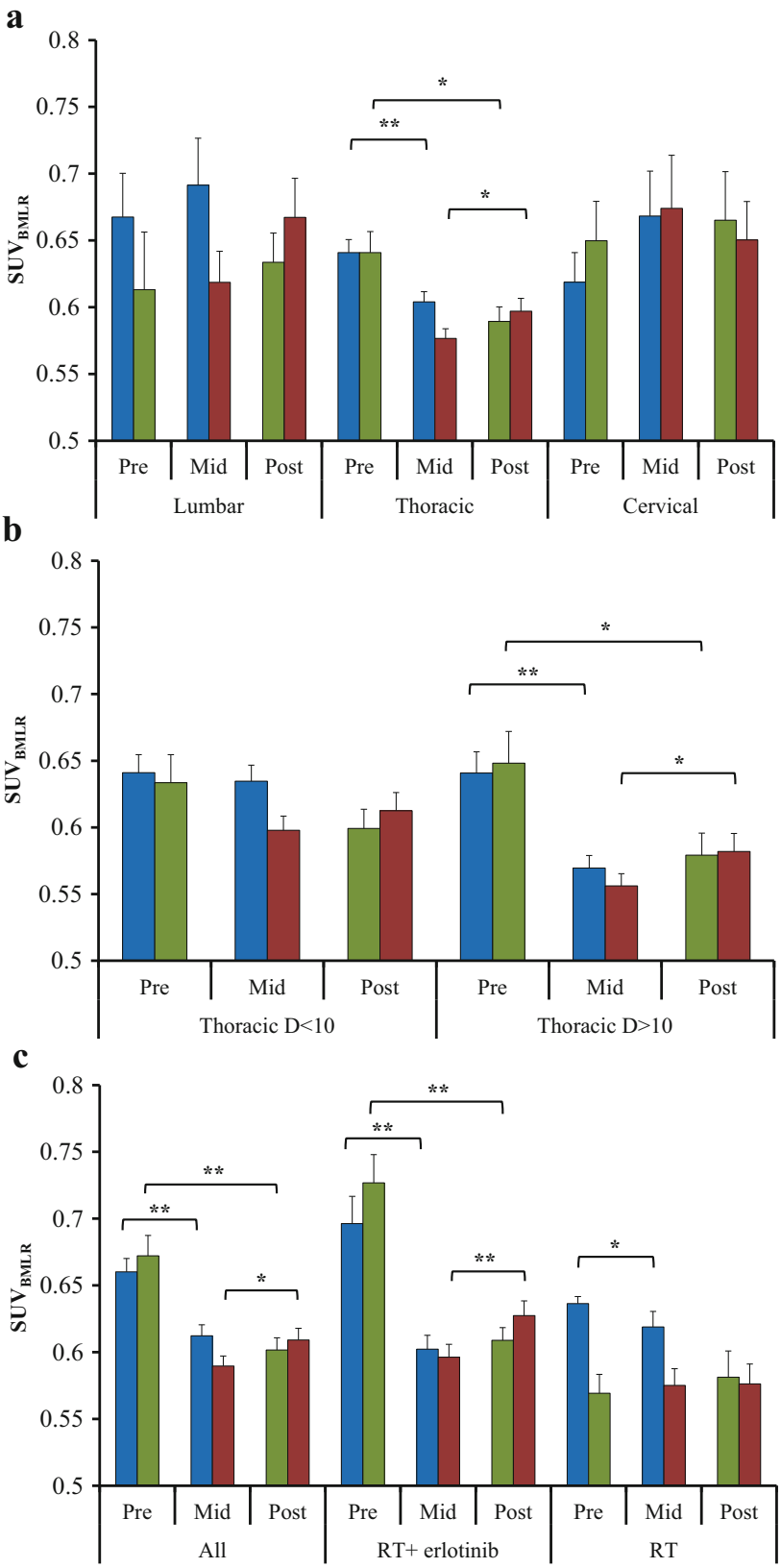

Fig. 4 Bar charts of the mean BM [^{18}F]FDG uptake corrected for liver at pre-, mid-, and post-therapy for **a** lumbar, thoracic, and cervical vertebrae, **b** thoracic vertebrae classified into low and high RT dose regions, and **c** vertebral column based on all population and treatment groups. Not all patients underwent all three PET examinations. Blue, green, and red colors represent SUV_{BMLR} from patients contributing to pre-mid, pre-post, and mid-post pairs of observations, respectively. The error bars correspond to 1 S.E.M. *p values < 0.05; **p values < 0.01.

treatment. Second, from pre-therapy to 6 weeks post-therapy, a reduction in SUV_{BMLR} was also evident. Third, an increase in BM metabolism was observed from 1 week into treatment to 6 weeks after completion of treatment. The reduction in the vertebral column [^{18}F]FDG uptake already after 1 week of treatment clearly results from high-dose irradiation of the thoracic vertebrae, as we did not identify any significant changes in the corresponding low-dose region or in the lumbar and cervical vertebrae (receiving low RT dose). Noticewala, et al. [22] reported that the volume of the functional thoracic vertebrae, defined by baseline [^{18}F]FDG PET, significantly increased due to a compensatory effect post CRT. An increasing trend, albeit not significant, in the [^{18}F]FDG uptake was indeed seen for the lumbar and cervical vertebrae after 1 week of treatment in our study. This could point to the compensatory effect similar to the findings by Noticewala, et al. [22], although the effect was not pronounced in our patient cohort.

Irradiation is reported to induce immunosuppression, for instance through BM ablation or stimulation of inhibitory cytokines [29]. Irradiation of the vertebrae may lead to apoptosis of hematopoietic stem cells, or cause a stop/delay in the proliferation or differentiation of hematopoietic stem cells. This may further result in a decrease in the blood cell counts and thus leads to hematologic toxicity in patients. Moreover, during thoracic RT a big portion of the blood pool is also irradiated as part of heart and aorta receive high dose of radiation. This may cause a depletion of the blood and further reduce hematopoietic stem cells pool size in addition to BM irradiation itself. In particular, due to high radiosensitivity of lymphocytes, lymphopenia may happen after only 1 week of treatment [30]. Hence, irradiation of the BM in the thoracic region and possibly irradiation of peripheral blood could reduce hematopoietic stem cells in the BM only after 1 week of RT. Part of the BM activity recovered 6 weeks post-treatment, but compared to pre-therapy, the BM activity was still significantly lower. This may imply that 6 weeks post-treatment is not adequate for BM to retain hematopoietic stem cell pool size. Higashi, et al. [31] reported that BM [^{18}F]FDG uptake in rodents transiently increased 1 day after delivery of 10 Gy compared to baseline level. The uptake then decreased significantly at day 9 after irradiation, which again was followed by an increase 18 days after irradiation. Moreover, the [^{18}F]FDG uptake in the un-irradiated part of the BM also increased at day 18 post-radiation. Apart from the transient increase in the [^{18}F]FDG uptake shortly after irradiation (which, to be detected, requires a PET scan maybe 3 days after start of RT), these findings are well in line with our findings.

Suppression of epidermal growth factor receptor (EGFR) activity, *via* drugs such as erlotinib, is reported to result in an increase in the mobilization of hematopoietic cells [32]. In our study, at the post-therapy session, vertebral column [^{18}F]FDG uptake was higher in patients receiving erlotinib in addition to RT compared to those receiving RT alone. In our previous work [25], we identified an elevation in the normal lung [^{18}F]FDG uptake for patients in the RT + erlotinib group at post-therapy. As we discussed [25], the elevated lung uptake may be due to an inflammatory response. Such an inflammatory response may also affect BM metabolism where it acts as a stimulant leading to a faster recovery of the BM activity in the RT + erlotinib group. We found a positive correlation between mean SUV in the lung and mean SUV in the vertebral column at post-therapy only for patients in the RT + erlotinib group. This could point to that the same EGFR-related mechanisms cause an elevation in both vertebral column and lung [^{18}F]FDG uptake 6 weeks after therapy for patients receiving erlotinib in addition to RT. In contrast, Doan, et al. [33] reported that erlotinib has an adverse effect on the regeneration of hematopoietic stem cells in mice following total body irradiation. Still, whether such effects are present in humans remain to be seen. Furthermore, total body irradiation will affect the entire blood pool, and may not be comparable to local RT. Moreover, the regulation of BM activity is mediated by various cytokines such as IL-6 [34]. We found a significant positive correlation between vertebral column [^{18}F]FDG uptake and IL-6 in patients receiving erlotinib. Erlotinib has been reported to induce the secretion of pro-inflammatory cytokines such as IL-6 in head and neck cancer cells [35]. The increase in the vertebral column activity post-therapy may be due to hematopoiesis recovery following RT stimulated by secretion of IL-6 by erlotinib. Still, we found that IL-6 levels in the RT group were higher than for RT + erlotinib group. Therefore, the role of IL-6 was not clear in our cohort of patients. Nevertheless, BM metabolism may result from cytokines produced by inflammatory responses, and cytokines produced by the neoplasm cannot be ruled out.

In conclusion, the RT dose-dependent BM [^{18}F]FDG uptake in the thoracic vertebrae may point to changes in the BM activity that may lead to a reduction in blood cells and hematologic toxicity after 1 week of RT. Pre-treatment [^{18}F]FDG PET did not reveal functional BM heterogeneity within the vertebral column. Systemic targeted treatment, such as erlotinib, in addition to RT, may cause an increase in the BM metabolism post-treatment. Although our results for the RT group are in line with the literature, the findings related to the use of erlotinib should be validated in an independent cohort.

Acknowledgements. We gratefully thank Ingerid Skjei Knudtsen, University of Oslo, Norway for her assistance in setting up the PET/CT protocol and data collection. This study was partly funded by the faculty of Mathematics and Natural Sciences, University of Oslo, Norway and was supported by the Norwegian Cancer Society and The regional health authorities in South East Norway.

Compliance with Ethical Standards. The study was approved by the Regional Committee for Medical and Health Research Ethics. A written informed consent was received from all patients.

Conflict of Interest

The authors declare that they have no conflict of interest.

References

1. Delaney G, Jacob S, Featherstone C, Barton M (2005) The role of radiotherapy in cancer treatment: estimating optimal utilization from a review of evidence-based clinical guidelines. Cancer 104(6):1129–1137

2. Begg AC, Stewart FA, Vens C (2011) Strategies to improve radiotherapy with targeted drugs. Nat Rev Cancer 11(4):239–253
3. van Baardwijk A, Bosmans G, Boersma L, Wanders S, Dekker A, Dingemans AMC, Bootsma G, Geraedts W, Pitz C, Simons J, Lambin P, de Ruysscher D (2008) Individualized radical radiotherapy of non–small-cell lung cancer based on normal tissue dose constraints: a feasibility study. Int J Radiat Oncol Biol Phys 71(5):1394–1401
4. Berg JM, Tymoczko JL, Stryer L (2006) Each organ has a unique metabolic profile. In: Biochemistry. W.H.Freeman & Co Ltd, New York, pp 851–854
5. Fan C, Hernandez-Pampaloni M, Houseni M, Chamroonrat W, Basu S, Kumar R, Dadparvar S, Torigian DA, Alavi A (2007) Age-related changes in the metabolic activity and distribution of the red marrow as demonstrated by 2-deoxy-2-[F-18]fluoro-D-glucose-positron emission tomography. Mol Imaging Biol 9(5):300–307
6. Dudek A, Mahaseth H (2005) Circulating angiogenic cytokines in patients with advanced non-small cell lung cancer: correlation with treatment response and survival. Cancer Invest 23(3):193–200
7. Colasante A, Mascetra N, Brunetti M et al (1997) Transforming growth factor beta 1, interleukin-8 and interleukin-1, in non-small-cell lung tumors. Am J Respir Crit Care Med 156(3):968–973
8. Patchen ML, MacVittie TJ, Williams JL, Schwartz GN, Souza LM (1991) Administration of interleukin-6 stimulates multilineage hematopoiesis and accelerates recovery from radiation-induced hematopoietic depression. Blood 77(3):472–480
9. Ramadori G, Van Damme J, Rieder H, Meyer zum Büschenfelde KH (1988) Interleukin 6, the third mediator of acute-phase reaction, modulates hepatic protein synthesis in human and mouse. Comparison with interleukin 1 p and tumor necrosis factor-a. Eur. J. Immuno 18:1259–1264
10. Deek MP, Benenati B, Kim S, Chen T, Ahmed I, Zou W, Aisner J, Jabbour SK (2016) Thoracic vertebral body irradiation contributes to acute hematologic toxicity during chemoradiation therapy for non-small cell lung cancer. Int J Radiat Oncol Biol Phys 94(1):147–154
11. Fairchild A, Harris K, Barnes E, Wong R, Lutz S, Bezjak A, Cheung P, Chow E (2008) Palliative thoracic radiotherapy for lung cancer: a systematic review. J Clin Oncol 26(24):4001–4011
12. Chen X, Liu Y, Røe OD, Qian Y, Guo R, Zhu L, Yin Y, Shu Y (2013) Gefitinib or erlotinib as maintenance therapy in patients with advanced stage non-small cell lung cancer: a systematic review. PLoS One 8(3):e59314
13. Hicks RJ, Kalff V, MacManus MP, Ware RE, Hogg A, McKenzie A, Matthews JP, Ball DL (2001) 18F-FDG PET provides high-impact and powerful prognostic stratification in staging newly diagnosed non-small cell lung cancer. J Nucl Med 42(11):1596–1604
14. Jiménez-Bonilla JF, Quirce R, Martínez-Rodríguez I, Banzo I, Rubio-Vassallo AS, del Castillo-Matos R, Ortega-Nava F, Martínez-Amador N, Ibáñez-Bravo S, Carril JM (2013) Diagnosis of recurrence and assessment of post-recurrence survival in patients with extracranial non-small cell lung cancer evaluated by 18F-FDG PET/CT. Lung Cancer 81(1):71–76
15. Gordon BA, Flanagan FL, Dehdashti F (1997) Whole-body positron emission tomography: normal variations, pitfalls, and technical considerations. AJR Am J Roentgenol 169(6):1675–1680
16. Lee JW, Seo KH, Kim E-S, Lee SM (2016) The role of 18F-fluorodeoxyglucose uptake of bone marrow on PET/CT in predicting clinical outcomes in non-small cell lung cancer patients treated with chemoradiotherapy. Eur Radiol 27(5):1912–1921
17. Rose BS, Liang Y, Lau SK, Jensen LG, Yashar CM, Hoh CK, Mell LK (2012) Correlation between radiation dose to ^{18}F-FDG-PET defined active bone marrow subregions and acute hematologic toxicity in cervical cancer patients treated with chemoradiotherapy. Int J Radiat Oncol Biol Phys 83(4):1185–1191
18. Liang Y, Bydder M, Yashar CM, Rose BS, Cornell M, Hoh CK, Lawson JD, Einck J, Saenz C, Fanta P, Mundt AJ, Bydder GM, Mell LK (2013) Prospective study of functional bone marrow-sparing intensity modulated radiation therapy with concurrent chemotherapy for pelvic malignancies. Int J Radiat Oncol Biol Phys 85(2):406–414
19. Franco P, Arcadipane F, Ragona R, Lesca A, Gallio E, Mistrangelo M, Cassoni P, Arena V, Bustreo S, Faletti R, Rondi N, Morino M, Ricardi U (2016) Dose to specific subregions of pelvic bone marrow defined with FDG-PET as a predictor of hematologic nadirs during concomitant chemoradiation in anal cancer patients. Med Oncol 33(7):72
20. Rose BS, Jee KW, Niemierko A, Murphy JE, Blaszkowsky LS, Allen JN, Lee LK, Wang Y, Drapek LC, Hong TS, Wo JY (2016) Irradiation of FDG-PET-defined active bone marrow subregions and acute hematologic toxicity in anal cancer patients undergoing chemoradiation. Int J Radiat Oncol Biol Phys 94(4):747–754
21. Yagi M, Froelich J, Arentsen L, Shanley R, Ghebre R, Yee D, Hui S (2015) Longitudinal FDG-PET revealed regional functional heterogeneity of bone marrow, site-dependent response to treatment and correlation with hematological parameters. J Cancer 6(6):531–537
22. Noticewala SS, Li N, Williamson CW et al (2017) Longitudinal changes in active bone marrow for cervical cancer patients treated with concurrent chemoradiation therapy. Int J Radiat Oncol Biol Phys 97(4):797–805
23. Hayman JA, Callahan JW, Herschtal A, Everitt S, Binns DS, Hicks RJ, Mac Manus M (2011) Distribution of proliferating bone marrow in adult cancer patients determined using FLT-PET imaging. Int J Radiat Oncol Biol Phys 79(3):847–852
24. Inoue K, Goto R, Okada K, Kinomura S, Fukuda H (2009) A bone marrow F-18 FDG uptake exceeding the liver uptake may indicate bone marrow hyperactivity. Ann Nucl Med 23(7):643–649
25. Abravan A, Eide HA, Knudtsen I, Løndalen A, Helland Å, Malinen E (2017) Assessment of pulmonary 18F-FDG-PET uptake and cytokine profiles in non-small cell lung cancer patients treated with radiotherapy and erlotinib. Clin Transl Radiat Oncol 4:57–63
26. Eide HA, Halvorsen AR, Sandhu V, et al. (2016) Non-small cell lung cancer is characterised by a distinct inflammatory signature in serum compared with chronic obstructive pulmonary disease. Clin Trans Immunol 5(11):e109. https://doi.org/10.1038/cti.2016.65
27. Mauch P, Constine L, Greenberger J, Knospe W, Sullivan J, Liesveld JL, Deeg HJ (1995) Hematopoietic stem cell compartment: acute and late effects of radiation therapy and chemotherapy. Int J Radiat Oncol Biol Phys 31(5):1319–1339
28. Hall EJ, Giaccia AJ (2006) Dose–response relationships for model normal tissues. In: Mitchell CW (ed) Radiobiology for the radiologist. Lippincott Williams & Wilkins, Philadelphia, pp 303–326
29. Formenti SC, Demaria S (2013) Combining radiotherapy and cancer immunotherapy: a paradigm shift. J Natl Cancer Inst 105(4):256–265
30. Heylmann D, Rödel F, Kindler T, Kaina B (2014) Radiation sensitivity of human and murine peripheral blood lymphocytes, stem and progenitor cells. Biochim Biophys Acta 1846(1):121–129
31. Higashi T, Fisher SJ, Brown RS, Nakada K, Walter GL, Wahl RL (2000) Evaluation of the early effect of local irradiation on normal rodent bone marrow metabolism using FDG: preclinical PET studies. J Nucl Med 41(12):2026–2035
32. Ryan MA, Nattamai KJ, Xing E, Schleimer D, Daria D, Sengupta A, Köhler A, Liu W, Gunzer M, Jansen M, Ratner N, le Cras TD, Waterstrat A, van Zant G, Cancelas JA, Zheng Y, Geiger H (2010) Pharmacological inhibition of EGFR signaling enhances G-CSF–induced hematopoietic stem cell mobilization. Nat Med 16:1141–1146
33. Doan PL, Himburg HA, Helms K, Russell JL, Fixsen E, Quarmyne M, Harris JR, Deoliviera D, Sullivan JM, Chao NJ, Kirsch DG, Chute JP (2013) Epidermal growth factor regulates hematopoietic regeneration following radiation injury. Nat Med 19(3):295–304
34. Bernad A, Kopf M, Kulbacki R, Weich N, Koehler G, Gutierrez-Ramos JC Interleukin-6 is required in vivo for the regulation of stem cells and committed progenitors of the hematopoietic system. Immunity 1(9):725–731
35. Fletcher EVM, Love-Homan L, Sobhakumari A, et al. (2013) Epidermal growth factor receptor inhibition induces pro-inflammatory cytokines via NOX4 in head and neck cancer cells. Mol Cancer Res